Mechanism of Hydrogen-Bond Array Isomerization in Tetrahydroxycalix[4]arene and Tetrahydroxythiacalix[4]arene

Jiří Matoušek,[†,||] Michal Čajan,[§] Petr Kulhánek,[†] and Jaroslav Koča*[,†,‡]

National Centre for Biomolecular Research and Institute of Chemistry, Faculty of Science, Kotlářská 2, Masaryk University, CZ-611 37 Brno, Czech Republic, and Department of Inorganic Chemistry, Palacký University, Křížkovského 10, CZ-779 00 Olomouc, Czech Republic

Received: October 23, 2007

Possible rearrangement mechanisms of hydrogen-bond arrays formed at the lower rim of tetrahydroxycalix[4]arene and tetrahydroxythiacalix[4]arene were studied by means of density functional theory and the resolution identity approximation modification of Møller-Plesset perturbation theory (RI-MP2). Influence of solvent to height of energy barriers was quantified by use of the conductorlike screening model (COSMO) of implicit solvent (chloroform). Generally, two types of mechanisms were investigated. The first is represented by a synchronous single-step jump of all four hydroxyl protons. Pathways of the second mechanism include the rotation of one or more hydroxyl groups around the C_{Ar}−O bond. Theoretical results, in agreement with recently published experimental data (Lang et al. *J. Chem. Phys.* **2005**, *122*, 044056), prefer a jump mechanism for the methylene-bridged calix[4]arene. Concerning the thiacalix[4]arene, results obtained by COSMO as well as RI-MP2 calculations show that the rotational mechanism is very competitive and it could even be more favorable.

Introduction

Hydrogen bonds and their networks play a fundamental role in the formation and stabilization of many biological as well as artificial supramolecular systems, and they strongly influence their function and properties. The correct view into the hydrogen-bond formation process as well as into other processes including the proton binding and transfer is essential for understanding reaction mechanisms and kinetics of these processes. Unfortunately, these processes are often characterized by small structural as well as energy changes, which make them quite complicated and difficult to follow by both experimental and theoretical approaches. Seen from this point of view, the well-known molecule calix[4]arene[1] (Figure 1) with its well-defined and rigid structure gives us an excellent and relatively simple model for understanding more complicated artificial as well as biomolecular hydrogen-bond networks and proton-transfer processes occurring within them.[2,3] For the same reasons, the molecule thiacalix[4]arene also may serve as a good model system.

Stability and flexibility of the molecular geometry of calix[4]arenes and thiacalix[4]arenes, host compounds with specific conic arrangement of the molecular structure, are strongly influenced by a number of hydrogen bonds, which can be formed within individual conformers (see Figure 1).[1,4−7] The stabilization effect is especially evident for the basic calix[4]arene system with completely nonsubstituted hydroxyl groups bound at the lower rim of the cavity. Such a system strongly prefers the *cone* arrangement in molecular structure, which is stabilized by a cyclic array of four strong hydrogen bonds

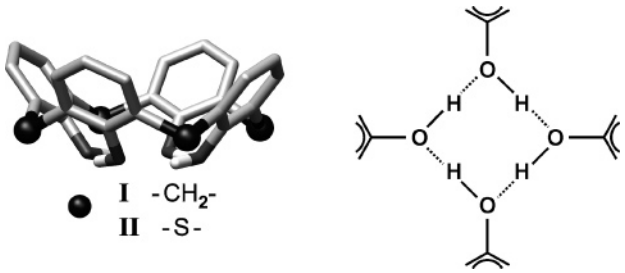

Figure 1. Cone conformer of calix[4]arene and thiacalix[4]arene molecules and arrangement of hydrogen-bond array at their lower rim.

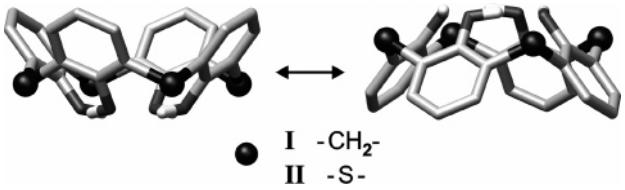

Figure 2. Cone−cone inversion of calix[4]arene molecules.

(Figure 1), the presence of which was confirmed, for example, by IR and NMR measurements.[8−10] Other stable conformations have not been observed in this case, although other experimental data, based mainly on the NMR spectroscopy, have shown that the cyclic system of hydrogen bonds is not absolutely rigid. When the hydrogen-bond network is broken, the rotation of phenyl rings around the bridges connecting them is allowed, and the molecule forms the identical inverse conical structure (Figure 2).[11,12] Another observed process is the fast flip-flop directional reorientation of hydrogen-bond arrays (Figure 3).[13−17] The molecular mechanism of this process is not yet clearly understood, and there are still questions whether this process is based just on proton tunneling through the hydrogen-bonding potential or on jumping of protons to their hydrogen-bonded oxygen neighbors without a conformational change on the

* Corresponding author: e-mail jkoca@chemi.muni.cz.
† National Centre for Biomolecular Research, Masaryk University.
‡ Institute of Chemistry, Faculty of Science, Masaryk University.
§ Palacký University.
|| Jiří Matoušek died during the final processing of the paper at the age of 28. The paper is dedicated to his memory.

10.1021/jp710236g CCC: $40.75
Published on Web 01/09/2008

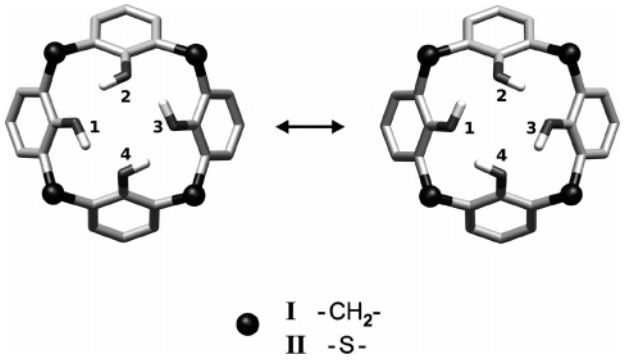

Figure 3. Flip-flop inversion between two possible arrangements of the hydrogen-bond array in a cone conformer of calix[4]arene (**I**) and thiacalix[4]arene (**II**) molecules. Hydroxyl groups are numbered for further descriptions of geometrical changes.

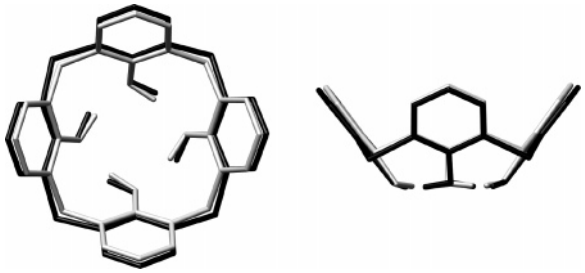

Figure 4. Comparison of B3LYP/cc-pVDZ optimized geometries of global minimum **M01** of calix[4]arene **I** (gray) and thiacalix[4]arene **II** (black).

C_{Ar}−O bonds, or if the reorientation is caused only by a conformational movement of hydroxyl groups around the C_{Ar}−O bond.

In the case of methylene-bridged calix[4]arene, kinetic studies based on temperature-dependent NMR measurements of ^{13}C nuclear spin transverse relaxation dependence on the effective radio frequency field provided rate constants in the range of (1.4×10^2)−$(4.2 \times 10^4\ s^{-1})$. Corresponding activation enthalpy and entropy are 8.8 kcal/mol and −8.4 cal/(mol·K), respectively.[16] In the case of thiacalix[4]arene, rate constants are in the range of (7.3×10^2)−$(1.7 \times 10^6)\ s^{-1}$, and the values of activation enthalpy and entropy are 9.2 kcal/mol and −3.6 cal/(mol·K), respectively.[17] Unfortunately, these experimental values do not provide any detailed information about the flip-flop inversion's mechanism and its reaction coordinate.

In this paper, we suggest several possible mechanisms of the above-mentioned hydrogen-bond array rearrangement, and we compare energy profiles of their reaction pathways by means of density functional theory (DFT) and Møller−Plesset perturbation theory in resolution identity approximation (RI-MP2).[18] Two principally different types of mechanisms have been studied. A jump mechanism represents a single-step synchronous transfer of all four hydrogens to the corresponding neighboring oxygen atoms. Rotational mechanisms are based on the rotation of hydroxyl groups around the C_{Ar}−O bond. Mechanisms of this type are generally more complicated, and they are realized via several transition states and less or more stable intermediates. The difference in behavior between normal methylene-bridged calix[4]arene and its thia analogue is also discussed. Calculated energy data are compared with those obtained from the above-mentioned dynamic NMR experiments published recently.[16,17]

Computational Details

Possible pathways of hydrogen-bond array reorganization in tetrahydroxycalix[4]arene **I** and its thia analogue **II** were explored by the DFT method. Hybrid functional B3LYP and cc-pVDZ basis sets were used. All calculations were done with TURBOMOLE 5.6[19] and GAUSSIAN 03[20] programs. Initial guesses of stationary points on the potential energy surface (PES) were found by the driving of specifically selected internal coordinates. In the case of a proton jump-based mechanism, O−H bond lengths were elongated, while in the case of a hydroxyl group rotation-based mechanism, O−H groups were rotated around C_{Ar}−O bonds. Estimated raw stationary point were then fully optimized and validated by vibrational analysis revealing all real frequencies for minima and only one imaginary frequency for the first-order transition states. Zero point corrections (ZPE), enthalpies and entropies were calculated for 298.15 K and 101.325 kPa.

Forming and breaking of hydrogen bonds play a key role in the studied problem and have to be described properly. Moreover, it is known that dispersion interactions between aromatic rings significantly affect the energetics of calix[4]arene conformers.[21,22] It is also known that DFT does not often correctly describe weak interactions. In order to make sure that the above energy contributions are properly treated and included, we have calculated single-point energies of optimized stationary points by the RI-MP2[18] method with a cc-pVDZ basis set. In the RI-MP2 method, 4-center 2-electron integrals are approximated by 3-center 2-electron integrals using optimized auxiliary basis functions. This leads to an enormous speed up of the calculations and significant savings in memory requirements when compared to the conventional MP2 method. With optimized auxiliary basis functions, RI-MP2 has been shown to almost identically reproduce conventional MP2 results.[23] To better take solvent influence into account, single-point energies were also calculated with *Conductor-like Screening Model* (COSMO) of a continuum solvent.[24]

In the text below, optimized structures are labeled according to their character on PES. Denotation of minima starts with **M** and those of transition states starts with **T**. Mirror structures are distinguished by suffixes **a** and **b**. Hydroxyl groups are labeled (see Figure 3) for easier description of geometrical changes, even if they are identical.

Results and Discussion

Hydroxyl groups in tetrahydroxycalix[4]arene form a unique hydrogen-bond array composed of four hydrogen bonds, that could be oriented either clockwise or counterclockwise (see Figure 3). Interconversion between these two structures (mirror images) was studied by NMR techniques, which show low free-energy barriers (11.29 kcal/mol for calix[4]arene and 10.32 kcal/mol for thiacalix[4]arene) and, more interestingly, different enthalpy and entropy contributions to the free energy barriers for calix[4]arene **I** and thiacalix[4]arene **II** (see Table 1).[16,17]

There have been several theoretical and experimental attempts to shed light on the mechanism of this rearrangement; however, all were unsuccessful until now. In this study we analyze the free-energy profile of two principally different types of possible isomerization mechanisms. A jump mechanism for calix[4]arene **I** was already discussed in the literature,[25] but only at an electronic energy level. It mostly serves as a reference for the jump mechanism of thiacalix[4]arene **II** or for rotational mechanisms of both calix[4]arene **I** and thiacalix[4]arene **II**. However, there are also other possible mechanisms including both jump and rotation events simultaneously. These mechanisms were not studied in this work, not only because of their extremely high complexity, but mainly because the proton jump in a disrupted hydrogen-bond network has to lead to ionic intermediates and, therefore, to higher energy barriers.

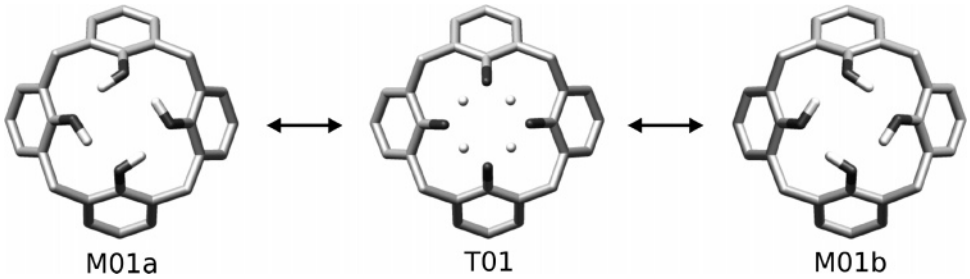

Figure 5. Jump mechanism for calix[4]arene **I**.

TABLE 1: Enthalpy, Entropy, and Free Energy Barriers of Reorganization of Hydrogen-Bond Arrays[a]

structure	ΔH, kcal/mol	ΔS, cal/(mol·K)	$T\Delta S$, kcal/mol	ΔG, kcal/mol
calix[4]arene	8.8	−8.4	−2.5	11.3
thiacalix[4]arene	9.2	−3.6	−0.9	10.3

[a] Measured by NMR for calix[4]arene and thiacalix[4]arene[16,17] at 298.15 K.

TABLE 2: Calculated Relative Energies and Selected Internal Coordinates for Optimized Stationary Points of Calixarene I[a,b]

	energy, kcal/mol							distance, Å	
structure	ΔE	ΔZPE	ΔH	$T\Delta S$	ΔG	ΔE(COSMO)	ΔE(RI-MP2)	$D1$	$D2$
M01	0.00	0.00	0.00	0.00	0.00	0.00	0.00	8.57	8.57
M02	12.04	−0.62	11.92	1.10	10.83	9.50	11.75	7.61	9.23
M03	14.12	−0.76	13.96	1.05	12.91	13.31	11.54	6.65	10.06
M04	17.39	−1.05	17.13	1.72	15.41	12.62	16.58	7.13	9.47
M05	19.35	−1.34	18.87	1.66	17.21	16.54	16.91	6.44	9.95
M06	21.24	−1.31	20.82	1.88	18.94	17.01	19.93	6.63	9.79
T01	16.80	−8.56	7.53	-1.82	9.35	17.24	16.97	8.87	8.87
T02	18.22	−0.95	17.45	-0.30	17.75	13.33	18.08	8.30	8.44
T03	14.85	−1.22	14.00	0.83	13.17	13.26	12.85	6.66	9.91
T04	18.34	−1.65	17.32	1.32	15.99	13.71	17.10	6.89	9.62
T05	12.08	−0.92	11.30	0.34	10.96	9.56	12.07	7.78	9.09
T06	20.53	−1.66	19.39	0.91	18.48	18.98	17.84	6.62	10.13
T07	19.46	−1.66	18.35	1.09	17.26	16.67	17.18	6.48	9.89
T08	22.52	−1.96	21.24	1.51	19.73	18.79	20.66	6.83	9.82
T09	18.61	−1.61	17.59	1.33	16.26	15.26	17.07	6.83	9.67
T10	14.33	−1.20	13.43	0.40	13.03	13.87	11.62	6.57	10.08
T11	21.37	−2.03	20.06	1.48	18.58	19.24	18.43	6.33	10.17
T12	22.94	−2.04	21.68	1.90	19.78	19.60	21.00	6.44	9.92
T13	21.87	−1.70	20.80	1.47	19.33	17.72	20.91	6.66	9.74

[a] ΔE, relative electronic energy; ΔZPE, relative zero-point energy; ΔH, relative enthalpy (calculated as the sum of ΔE, ΔZPE, and thermal corrections to enthalpy at 298.15 K and 101.325 kPa); $T\Delta S$, relative entropy contribution at 298.15 K and 101.325 kPa; ΔG, relative free energy (calculated as the sum of ΔH and $-T\Delta S$). The B3LYP/cc-pVDZ optimized structures were used for single-point energy calculations by use of B3LYP/cc-pVDZ with a chloroform COSMO model and RI-MP2/cc-pVDZ [corresponding relative electronic energies are ΔE(COSMO) and ΔE(RI-MP2)]. Influence of the solvent is exhibited by comparison of ΔE with ΔE(COSMO), while importance of proper evaluation of weak interactions is seen from comparison of ΔE with ΔE(RI-MP2). Distances $D1$ and $D2$ between carbon atoms in para positions of opposite aromatic rings are presented as a measurement of cavity deformation; values are taken from the structures optimized by B3LYP/cc-pVDZ. [b] The chiral parts of conformational space are bridged by achiral **T04** and **T06** and chiral **T09** transition states. For details about minima and transition states, see text.

Comparison of Calix[4]arene I and Thiacalix[4]arene II Geometries. Calix[4]arene and thiacalix[4]arene are structural analogues, and their cone conformers have quite similar overall shapes (see Figure 4) and conical arrangements of the cavity. However, detailed structural analysis reveals differences in geometrical parameters characterizing either the whole cavity or hydrogen bonding at the lower rim. Values presented here are taken from geometries optimized with B3LYP/cc-pVDZ.

The distance between adjacent aromatic carbon atoms of the thiacalix[4]arene upper rim (9.08 Å) is greater than that for calix[4]arene **I** (8.57 Å). Bond angle $C_{Ar}-S-C_{Ar}$ is more acute in the case of thiacalix[4]arene **II**, 103.8° in comparison to 113.8° for $C_{Ar}-CH_2-C_{Ar}$ of calix[4]arene **I**. The length of the hydrogen bond and O−H···O angle are 1.86 Å and 149.4° for thiacalix[4]arene compared to 1.68 Å and 163.9° for the calix[4]arene. Both values indicate stronger hydrogen-bonding capability in calix[4]arene **I**.

Calix[4]arene (I) Jump Mechanism. *B3LYP/cc-pVDZ.* In this mechanism, two global minima (**M01a** and **M01b**) of the calix[4]arene molecule with C_4 symmetry, differing in direction of hydrogen-bond arrays, are connected by the transition state **T01** with C_{4v} symmetry (see Figure 5). In the transition state, hydrogen atoms of hydroxyl groups are situated exactly in the middle between adjacent oxygen atoms, and reorganization can be interpreted as a synchronous jump of all four protons. Calculated enthalpy and free energy barrier are 7.53 and 9.35 kcal/mol, respectively (Table 2). Employment of COSMO solvation model provides a higher electronic energy barrier by 0.44 kcal/mol. All calculated data are in relatively good agreement with experimental NMR data (see Tables 1 and 2).

TABLE 3: Calculated Relative Energies and Selected Internal Coordinates for Optimized Stationary Points of Calixarene II[a]

	energy, kcal/mol							distance, Å	
structure	ΔE	ΔZPE	ΔH	$T\Delta S$	ΔG	ΔE(COSMO)	ΔE(RIMP2)	*D*1	*D*2
M01	0.00	0.00	0.00	0.00	0.00	0.00	0.00	9.08	9.08
M02	10.48	−0.07	10.66	0.78	9.88	8.39	8.77	6.92	10.38
M03	13.41	−0.18	13.59	1.15	12.44	10.74	11.68	6.58	10.44
M04	13.73	−0.21	13.91	1.28	12.63	10.77	11.91	6.53	10.40
M05	17.14	−0.23	17.28	1.24	16.05	14.21	14.62	6.08	10.65
TI01	23.03	−9.66	12.80	−0.85	13.64	22.98	22.79	9.55	9.55
T02	16.65	−0.90	15.92	0.96	14.97	14.07	14.98	6.66	10.65
T03	21.45	−0.82	20.78	0.67	20.11	17.55	18.94	6.43	10.52
T04	14.62	−0.67	14.03	0.43	13.60	12.91	11.78	6.49	10.66
T05	16.40	−0.67	15.82	0.44	15.38	12.10	14.59	6.96	10.29
T06	18.97	−0.94	18.25	0.94	17.30	15.62	16.01	6.55	10.43
T07	20.17	−0.96	19.38	0.68	18.70	17.18	16.20	5.76	10.78
T08	19.53	−0.91	18.81	1.14	17.68	15.51	17.46	6.25	10.60
T09	14.77	−0.78	14.10	0.65	13.45	12.64	11.96	6.63	10.49

[a] See footnote *a* in Table 2.

The relative electronic energy of **T01** (16.80 kcal/mol) in vacuum and its calculated geometry are in agreement with previously published data.[25] Agreement with experimental NMR data is achieved when ZPE correction (−8.56 kcal/mol) is included.

Thiacalix[4]arene (II) Jump Mechanism. *B3LYP/cc-pVDZ.* Concerning the proton jump mechanism, the situation is different and more complicated compared to calixarene **I** behavior. Data are collected in Table 3. The C_{4v} symmetrical structure **T01** was found to be the transition state of the third order. There are two structures close to **T01** that exhibit only one imaginary frequency in vibration analysis and can therefore serve as estimates of real transition states. Both can be considered to be "internal ions". The first (**TI01**) has positive charge $-OH_2^+$ and negative charge $-O^-$ on opposite oxygen atoms and exhibits a relative free energy of 13.64 kcal/mol (see Figure 6). The second structure (**TI02**) has positive charge $-OH_2^+$ localized on one oxygen atom and a negative charge $-O^-$ on the neighboring one. Contrary to **TI01**, fully optimized stationary point **TI02** was not found. Electronic energies of all three structures (**T01**, **TI01**, and **TI02**) are very close, and there exists a very flat plateau on the PES around them. It is realistic to expect that the jump mechanism proceeds via this plateau.

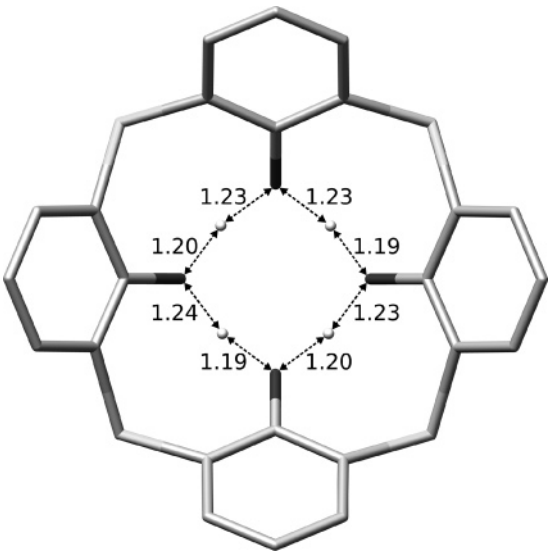

Figure 6. Geometry of nonsymmetrical transition state **TI01** of thiacalix[4]arene **II** with highlighted interatomic distances (Å) in hydrogen-bond array.

Unfortunately, detailed analysis of this plateau and refinement of a real transition-state geometry probably requires the use of highly accurate post-Hartree−Fock methods with a large basis set that goes beyond the efforts of this paper. Agreement between experimental and calculated free energy was not as comparable as the calixarene **I** (refer to Tables 1 and 3), even if the agreement with experimental entropy was excellent.

The above-described dissimilarities between the proton jump mechanism for calix[4]arene **I** and that for its thia analogue **II** can be explained by differences in their geometries (see section Comparison of Calix[4]arene **I** and Thiacalix[4]arene **II** Geometries) and by different electron distributions. Primarily, hydrogen bonds in thiacalix[4]arene do not have such convenient geometry and are therefore weaker. The complicated character of the PES around the **T01** of thiacalix[4]arene can also be caused by the fact that hydroxyl hydrogens at the lower rim can interact not only with oxygen atoms but also with bridging sulfur atoms.[8] These results have motivated us to investigate alternative pathways based on rotation of hydroxyl groups around $C_{Ar}-O$ bonds.

Calix[4]arene Rotational Mechanisms. *B3LYP/cc-pVDZ.* Conformational space of calixarene **I** was explored by the rotation of hydroxyl groups around $C_{Ar}-O$ bonds and six stable local minima were found (see Figure 7 and Table 2). These stationary structures have some hydroxyl groups turned out from the cavity, and hence the corresponding hydrogen-bond array is not complete. Formation of such minima is usually accompanied by deformation of the cavity to the pinched cone conformation. This conformation, where distances between opposite aromatic rings are not equal, is known to be preferable for calix[4]arenes with substituted hydroxyl groups at the lower rim, for example, by alkoxy groups.[21,22] A hydrogen-bond array in such systems can also be broken or not formed at all. Possible transition states connecting these local minima either mutually or with both global minima were found. Consequently, we propose several mechanisms of hydrogen-bond array reorganizations leading from one global minimum to another. An overall scheme of possible pathways is shown in Figure 7. Main energy and geometric characteristics of stationary points are summarized in Table 2.

Three local minima can be reached from the starting global minimum **M01a** by rotation of one hydroxyl group. For example, rotation of the OH-1 group (for numbering see Figure 3) out from the cavity leads to the **M02a** minimum with a relative free energy of 10.83 kcal/mol. The hydrogen-bond array

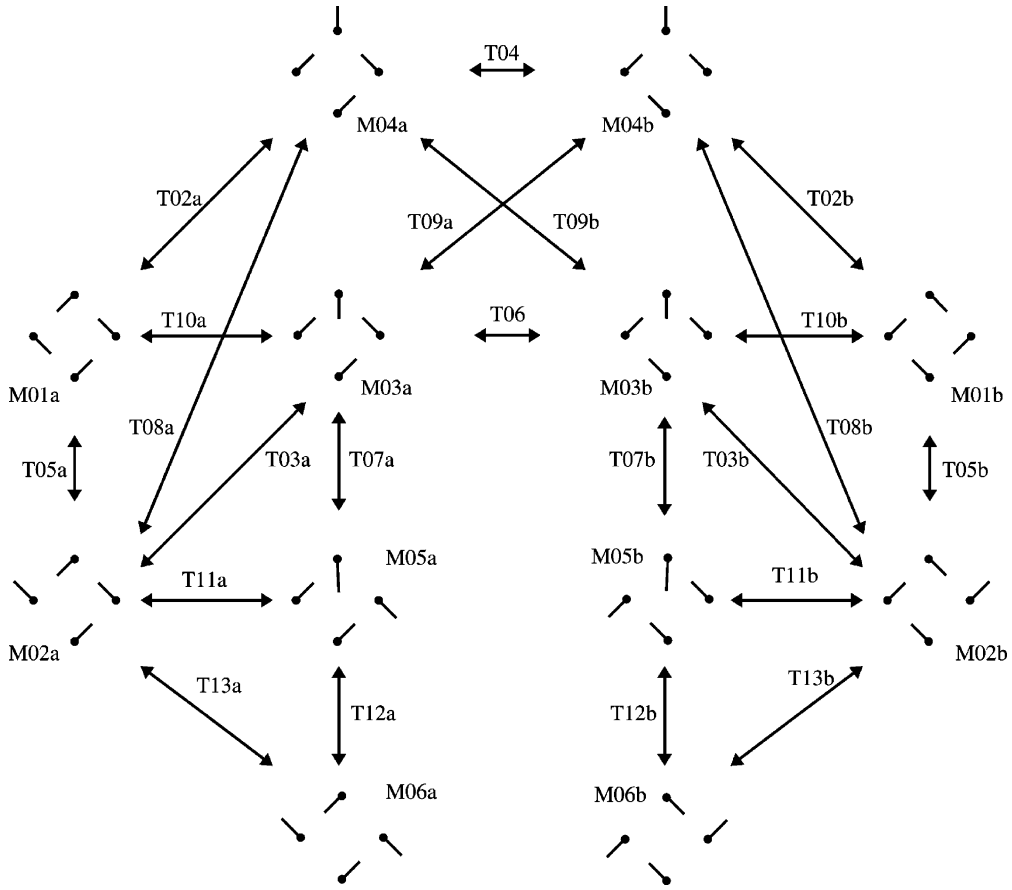

Figure 7. Proposed pathways for reorganization of hydrogen-bond array in calixarene **I,** based on hydroxyl group rotations. Minima are displayed as hydrogen-bond arrays in a schematic way (hydroxyl groups are visualized as a point for the oxygen and line for the OH bond). For further data see Table 2.

is partially broken, and only three hydrogen bonds contribute to the stabilization of the cone geometry. This rotation proceeds via the transition state **T05a** (10.96 kcal/mol). Further rotation of OH-1 group brings the molecule from a **M02a** minimum to **M03a** minimum (12.91 kcal/mol) via transition state **T03a** (13.17 kcal/mol). During this process, the OH-1 group pushes the neighboring OH-2 group inward the cavity. Similar to the **M02a** minimum, the **M03a** structure is also stabilized by three hydrogen bonds. However, the two of them are formed by the same oxygen atom.

On the contrary, when the transformation of **M01a** starts with rotation of OH-1 group in the opposite direction, through the inner part of the cavity, the molecule changes the geometry to minimum **M04a** (15.41 kcal/mol) via transition state **T02a** (17.75 kcal/mol). Also in this case, rotating OH-1 group causes interaction with the neighboring OH-2 group and pushes it out from the cavity. The **M04a** minimum is an analogue of the **M03a** structure and its geometry is also stabilized by three hydrogen bonds. Two of them share one oxygen atom. The hydrogen bound to this oxygen points to the outside of the cavity (for a better view, see Figure 7).

Both **M03a** and **M04a** structures are key intermediates on the pathways connecting global minima **M01a** and **M01b**. Rotation of one hydroxyl group (OH-4) leads to their mirror images, minima **M03b** and **M04b**, respectively. In the case of the **M03a**−**M03b** transition, the OH-4 group rotates outside the cavity via transition state **T06** (18.48 kcal/mol). In the case of the **M04a**−**M04b** transition, the same group rotates through the inner part of the cavity via transition state **T04** (15.99 kcal/mol).

In the conformational space searched, another three pathways connecting the key minima exist. These are **M03a** with **M04b**, **M02a** with **M04a**, and **M03a** with **M01a** (Figure 7). The first of them is the most important, because it represents the third direct connection between **a** and **b** mirror parts of the conformational space. Minimum **M03a** is connected with the **M04b** structure by rotation of the OH-2 group in the direction of the OH-3 group that is pushed out from the cavity. Relative free energy of the transition state of this rearrangement, **T09a**, is 16.26 kcal/mol. **M02a** structure can be transformed into the **M04a** via the transition state **T08a** (19.73 kcal/mol) by rotation of the OH-4 group outside the cavity. Minima **M01a** and **M03a** are directly connected by transition state **T10a** (13.03 kcal/ mol). This transformation should not be simply interpreted as a single dihedral angle rotation but rather as a synchronous movement.

In addition to local minima exhibiting only one broken hydrogen bond in the array, two types of minima with two broken hydrogen bonds were found. First, **M06a** (18.94 kcal/mol) is connected with minimum **M02a** by a rotation of the OH-3 group outside the cavity. This rotation proceeds via transition state **T13a** (19.33 kcal/mol). The second one, minimum **M05a** (17.21 kcal/mol), is then obtained from **M06a** via transition state **T12a** (19.78 kcal/mol). Structure **M05a** is very unstable and undergoes a conversion to another two local minima: **M03a** via transition state **T07a** (17.26 kcal/mol) and **M02a** minimum via transition state **T11a** (18.58 kcal/mol). As seen in Figure 7, most of these interconversions cannot be described as a single dihedral movement but rather characterized as synchronous movements.

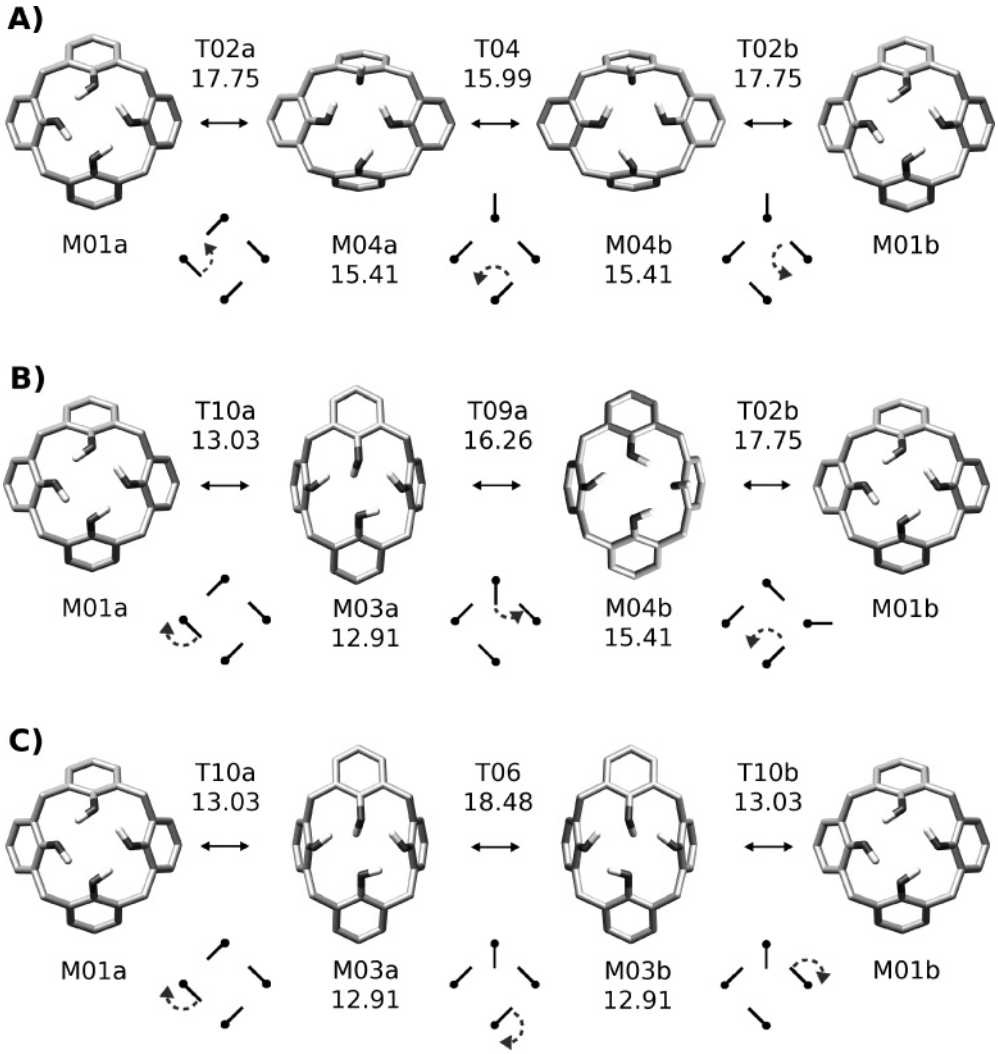

Figure 8. Three energetically preferable rotational mechanisms for calix[4]arene **I**. Energies are expressed in kilocalories per mole. For further details see Table 2 and Figure 7.

Solvent Effects. It is realistic to expect that exposure of polar hydroxyl groups to a nonpolar solvent, in which studied calixarenes are soluble, can strongly influence interconversion energy barriers. To explore the quantity of these solvation contributions, we have calculated single-point energies of optimized stationary points using the COSMO model and compared them to those obtained in vacuum. Energies calculated by this approach are summarized in Table 2. It implies that calculations with the continuum chloroform model generally provide lower heights of energy barriers of rotational mechanisms compared to those obtained by calculations in the vacuum. In contrast, jump mechanisms exhibit a higher energy barrier in continuum solvent than in vacuum.

RI-MP2/cc-pVDZ. Rearrangement of hydrogen-bond arrays in calix[4]arene **I** often causes significant differences in the shape of the cavity (Table 2). Stability of hydrogen bonds and $\pi-\pi$ interactions between opposite aromatic rings thus should be significantly different for different stationary points on the PES. Therefore, single-point energies on the RI-MP2/cc-pVDZ level were calculated in order to describe these weak interactions more precisely. Calculated values are shown in Table 2. The values show that the more pinched the cavity is, the more significant the dispersion interaction between the opposite aromatic rings is and, consequently, the more significant the difference between DFT and RI-MP2 energy is. This trend is nicely exhibited by comparison of geometries and energies of stationary points, for example **M01** with **M04** and **T02** with **T10** (see also the distances *D*1 and *D*2 in Table 2).

Proposed Mechanisms. Four mechanisms for reorganization have been proposed as energetically most convenient on the B3LYP/cc-pVDZ level. The first represents the proton jump (**M01a-T01-M01b**), and it is a single-step mechanism. The other three mechanisms are based on rotations of hydroxyl groups around the $C_{Ar}-O$ bond and each of them comprises three steps. These are (A) **M01a-T02a-M04a-T04-M04b-T02b-M01b**, (B) **M01a-T10a-M03a-T09a-M04b-T02b-M01b**, and (C) **M01a-T10a-M03a-T06-M03b-T10b-M01b** (see Figure 8). The jump mechanism has a global free energy barrier of 9.35 kcal/mol. The rotational mechanisms A, B, and C have global barriers of 17.75, 17.75, and 18.48 kcal/mol, respectively. Note that calculated solvent effects decrease energy barriers on pathways of rotational mechanisms, while the transition state of the jump mechanism has higher energy in continuum solvent; also, the RI-MP2 calculations indicate that energy barriers of rotational mechanisms could be lower according to dispersion interactions. Nevertheless, it can be concluded that in nonpolar solvents the jump mechanism is dominant. Enthalpy and free energy barriers of the jump mechanism calculated in a vacuum show good agreement with NMR experiment results; this agreement is even better if the solvent effect is taken into account. The rotational

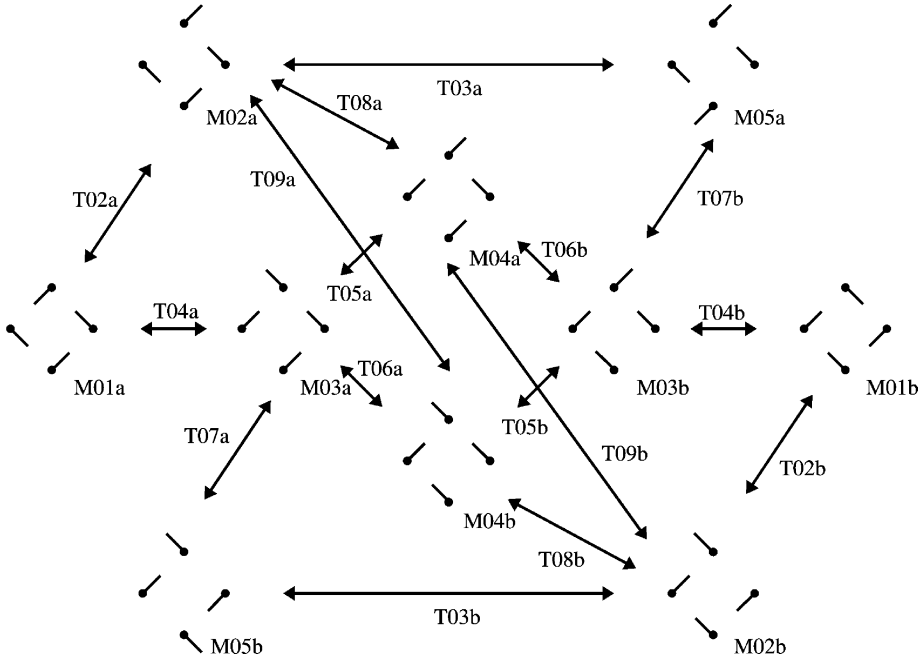

Figure 9. Proposed rotational mechanisms of the reorganization of hydrogen-bond arrays in thiacalix[4]arene **II**. Minima are displayed as hydrogen-bond arrays in a schematic way (hydroxyl groups are visualized as points for oxygen and lines for OH bonds).

mechanisms remain less favorable in nonpolar environment than the jump mechanism, although more testing in polar solvents should be considered.

Thiacalix[4]arene Rotational Mechanisms. *B3LYP/cc-pVDZ.* Conformational space of hydroxyl group rotations was again explored by single-coordinate driving. Five local minima as well as transition states connecting them were found. Conformational space based on hydroxyl-group rotations was quite different in comparison to the behavior of calixarene **I**. Calixarene **II** has a larger cavity, and hence longer hydrogen bonds, resulting in lower steric requirements for hydroxyl groups turning out from the array. Similar minima differing in spatial orientation of hydroxyl groups toward the calixarene cavity can be formed (Figure 9). Moreover, when one or two hydroxyl groups are turned out from the array, the cavity is more deformed to a pinched cone shape than it is in analogous structures of calix[4]arene **I**. Main structural and energy characteristics of collected stationary points are summarized in Table 3.

Two local minima can be reached from the **M01a** minimum by rotation of one hydroxyl group. The first, **M02a** with relative free energy 9.88 kcal/mol, is separated by transition state **T02a** (14.97 kcal/mol), and a corresponding OH-2 group rotates through the outer part of the cavity. The geometry of the **M02a** minimum is stabilized by three hydrogen bonds, and one hydroxyl group is turned out from the calixarene cavity. The second minimum, **M03a** (12.44 kcal/mol), is formed from **M01a** by rotation of the OH-1 group through the inner part of the cavity. The neighboring OH-2 group is simultaneously pushed out of the cavity. Also in this case, three hydrogen bonds stabilize the geometry. Two of them are made by the same oxygen atom. Conformational change proceeds via the transition state **T04a** (13.60 kcal/mol).

Another two minima, **M04a** and **M04b**, resulted from the single rotation of one hydroxyl group of the **M03a** minimum. These minima are mirror images with relative free energy 12.63 kcal/mol. Flipping of the OH-2 group through the outer part of the cavity to the opposite side changes the geometry of the molecule via transition state **T05a** (15.38 kcal/mol) to minimum **M04a** (see Figure 9). In addition to this pathway, rearrangement of molecular geometry can also proceed via rotation of the opposite OH-4 group through the inner part of the cavity. In this case, movement via transition state **T06a** (17.30 kcal/mol) leads to the minimum **M04b**. Furthermore, the **M03a** structure is connected with the **M05b** minimum (16.05 kcal/mol) by transition state **T07a** (18.70 kcal/mol). To make this interconversion, the OH-3 group rotates through the inner part of the cavity, and on the contrary, the neighboring OH-4 group is pushed out. Consequently, minimum **M05b** has two hydroxyl groups pointing out from the cavity, and hence it is stabilized by only two hydrogen bonds.

In the conformational space searched, three other pathways starting from previously mentioned minimum **M02a** were found. Rotation of the OH-4 group through the outer part of the cavity leads via transition state **T03a** (20.11 kcal/mol) to the minimum **M05a**. The remaining two pathways lead to minima **M04a** and **M04b**, respectively. Pathway between **M02a** and **M04a** structures is carried out by rotation of the OH-1 group through the inner part of the cavity via transition state **T08a** (17.68 kcal/mol). Transformation of the **M02a** minimum to the **M04b** minimum requires rotation of the OH-3 group through the inner part of cavity via transition state **T09a** (13.45 kcal/mol).

Solvent Effects. Single-point energies were calculated by use of the continuum solvation model COSMO, similarly as in the case of calixarene **I**. Exposure of hydroxyl groups to chloroform provides even lower energies of stationary points compared to those from vacuum calculations (see Table 3). Energy barriers for rotational mechanisms, which always proceed via such stationary points, are therefore lower in chloroform than in vacuum.

RI-MP2/cc-pVDZ. Changes in hydrogen-bond arrays often cause significant differences in shape of the cavity also in the case of calixarene **II**. Generally, the thiacalixarene cavity has a more pinched shape, and π-systems of opposite pinched aromatic rings interact more intensively, contrary to the analogous situation in the methylene-bridged system. Thus, single-point energies at the RI-MP2/cc-pVDZ level were calculated to cover electron correlation effects. The energy

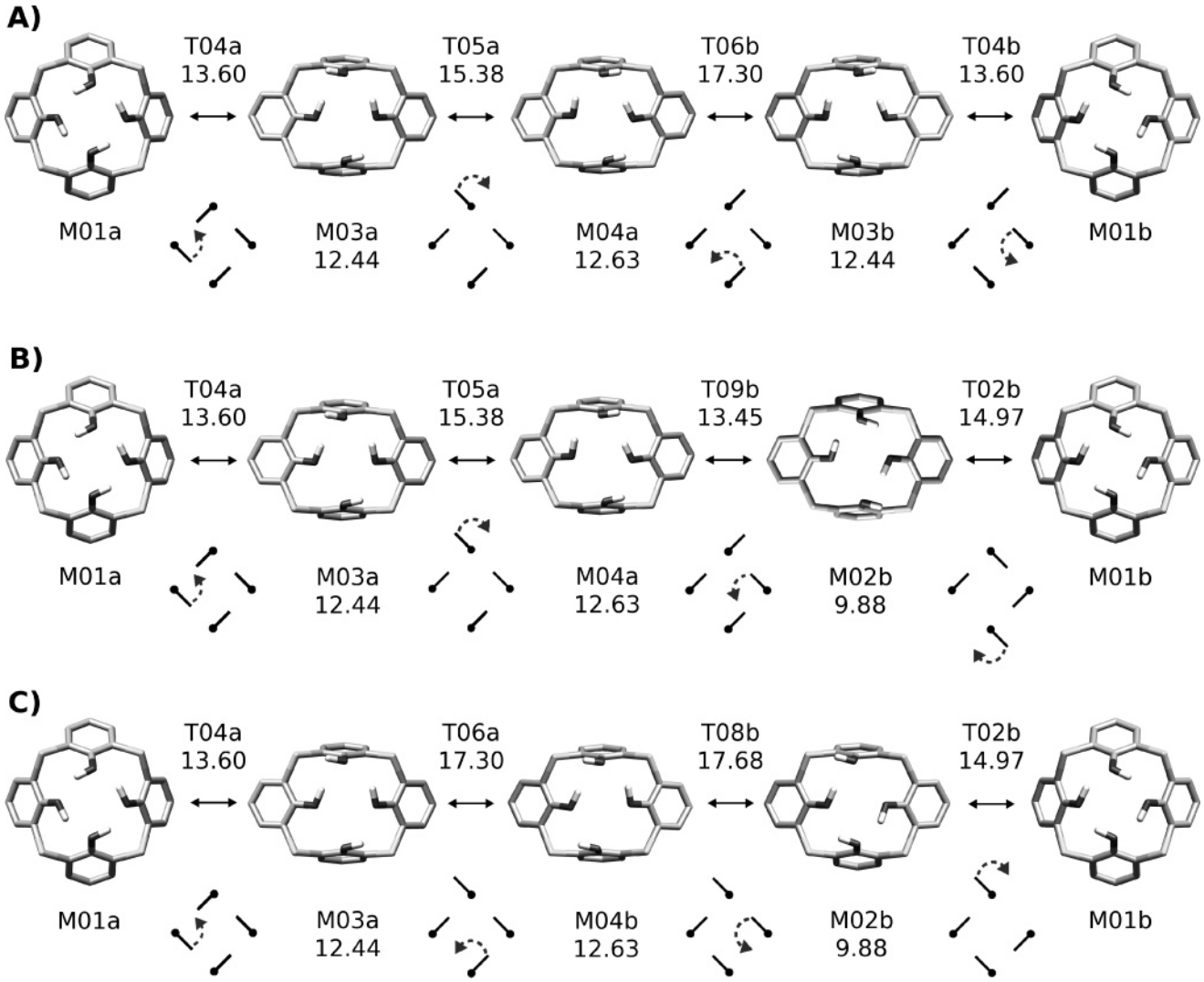

Figure 10. Three energetically preferable rotational mechanisms for thiacalixarene **II**. Energies are in kilocalories per mole. For further details see Table 3 and Figure 9.

values are shown in Table 3. Due to the stabilizing influence of $\pi-\pi$ interactions, the height of energy barriers for rotational mechanisms is lower when calculated on a RI-MP2 level. To form a better idea of this trend, energies in Table 3 calculated for stationary points should be compared, for example, **M01** with **M03** and **TI01** with **T02** (for the shape of the cavity see distances *D*1 and *D*2).

Proposed Mechanisms. Even if the pathway for the jump mechanism is not absolutely clear, it can be concluded that most probably it proceeds via a plateau represented by transition state **TI01** (13.64 kcal/mol). Additionally, a number of mechanisms based on rotations of hydroxyl groups can be also proposed on the basis of B3LYP/cc-pVDZ analysis. Three most energetically convenient mechanisms are described herein and are compared with a competitive jump mechanism. These are (A) **M01a-T04a-M03a-T05a-M04a-T06b-M03b-T04b-M01b**, (B) **M01a-T04a-M03a-T05a-M04a-T09b-M02b-T02b-M01b**, and (C) **M01a-T04a-M03a-T06a-M04b-T08b-M02b-T02b-M01b** (see Figure 10). Each of these three mechanisms consists of four steps, and they differ in their global barriers. Mechanism A has a global barrier of 17.30 kcal/mol, mechanism B exhibits a global barrier of 14.97 kcal/mol, and mechanism C demonstrates the highest global barrier of 17.68 kcal/mol. The effect of solvent is similar to the calixarene **I** case, and it generally decreases the height of rotational mechanism barriers. Results of RI-MP2 calculations indicate attractive dispersion interaction between aromatic rings, which is more important when the cavity of calixarene is deformed (pinched). Calculated lower energy values of such structures, in comparison with those obtained by DFT, correspond with this fact. This occurs again in the case of stationary points on rotational pathways. Therefore, it is difficult to decide which type of mechanism is dominant in the case of the thiacalix[4]arene. The global free-energy barrier of the optimal rotational mechanism (B) is given by the relative free energy of transition state **T02** (14.97 kcal/mol), which is a value comparable to that for the jump mechanism (13.64 kcal/mol). Moreover, electronic energy of this transition state is strongly influenced (decreased) either by the solvent effect or by intramolecular $\pi-\pi$ interactions. These effects could be so intensive that it can make this rotational mechanism more preferable to the jump mechanism (compare energy values in Table 3), even if the value of entropy contribution to the free energy barrier obtained by NMR experiments agrees rather with the jump mechanism. However, the entropic balance of rotational mechanism can be different in solvent. Rotation around the $C_{Ar}-O$ bonds also can be facilitated by larger cavity and lower sterical requirements for hydroxyl group movement. Possible stabilization effects of weak interactions between hydroxyl hydrogens and sulfur bridges should eventually be taken into account also. Nevertheless, quantification of such

contributions requires a detailed analysis of free energy surfaces by highly accurate correlated QM methods.

Conclusions

In this paper, the configurational and conformational space of cyclic hydrogen-bond arrays formed at the lower rim of tetrahydroxycalix[4]arene **I** and tetrahydroxythiacalix[4]arene **II** molecules was explored in detail by means of DFT and RI-MP2 calculations. Basically, two identical arrangements of hydrogen-bond arrays can exist, depending on the orientation of hydrogen bonds. Several molecular mechanisms of interconversion of these two geometries were proposed. These pathways belong to two principally different groups. The first group comprises proton jump mechanisms, while the second one is composed of mechanisms based on the rotation of hydroxyl groups. Solvent effects were quantified by use of a COSMO implicit solvation model. Proper investigation of intramolecular weak interactions was performed by the RI-MP2 method. Obtained results of computational analysis were compared to recently published experimental NMR data.[16,17]

In the case of methylene-bridged calix[4]arene **I**, the single-step proton jump mechanism with a calculated free energy barrier of 9.35 kcal/mol was compared with three proposed rotational mechanisms, all of which had higher global free energy barriers of 17.75, 17.75, and 18.48 kcal/mol. Each of them comprises three steps. Values of enthalpy (7.53 kcal/mol) and free energy (9.35 kcal/mol) barriers of the jump mechanism calculated in a vacuum were in agreement with values obtained by NMR experiment measurements (enthalpy barrier 8.8 kcal/mol, free energy barrier 11.3 kcal/mol). This agreement is even better if the solvent effect is taken into account. It can clearly be concluded that the jump mechanism is dominant for the reorganization of hydrogen-bond arrays of calix[4]arene **I** in nonpolar solvent, although rotational mechanisms should still be considered and tested in polar solvents.

Two transition states were determined for jump mechanisms in the thiacalix[4]arene **II**: (a) symmetrical (C_4) transition state of the third order and (b) energetically very similar nonsymmetrical transition state of the first order (relative free energy of 13.64 kcal/mol, relative enthalpy of 12.80 kcal/mol). These structures are located on a very flat plateau on the PES. From this point of view, the proton jump pathway is most likely carried out either as a single-step mechanism based on a synchronized four-proton jump or as more complicated multistep process. Agreement with experimental enthalpy (9.2 kcal/mol) and free energy (10.3 kcal/ mol) barrier is not as evident as in the case of calixarene **I**. Furthermore, three energetically reasonable pathways based on rotational mechanisms were proposed with global free energy barrier heights of 14.97, 17.30, and 17.68 kcal/mol. All of them are four-step mechanisms. When solvent effects and effects of dispersion $\pi-\pi$ interaction on energy barrier heights are taken into account, it can be concluded that a rotational mechanism can be very competitive or even the dominant mechanism. Thus, the rotational mechanism is a much more important alternative to the jump mechanism than in the case of the calix[4]arene **I**.

Acknowledgment. We thank the Supercomputing Centre in Brno, Czech Republic, for providing access to computer facilities. Financial support from the Ministry of Education, Youth, and Physical Training of the Czech Republic (Contract MSM0021622413 −to P.K. and LC06030 −to J.K.), the Grant Agency of the Czech Republic (Grant 204/03/H016 −to J.M.), and the Grant Agency of the Academy of Sciences of the Czech Republic (Grant IAA400200503 −to M.C.) is gratefully acknowledged.

References and Notes

(1) *Calixarenes 2001*; Asfari, Z., Böhmer, V., Harrowfield, J., Vicens, J., Eds.; Kluwer Academic Publishers: Dordrecht, The Netherlands, 2001.

(2) For example: (a) Ohmine, I.; Saito, S. *Acc. Chem. Res.* **1999**, *32*, 741−749. (b) Smith, J. D.; Cappa, C.D.; Wilson, K. R.; Messer, B. M.; Cohen, R. C.; Saykally, R. J. *Science* **2004**, *306*, 851−853.

(3) For example: (a) Trylska, J.; Grochowski, P.; McCammon, J. A. *Protein Sci.* **2004**, *13*, 513−528. (b) Ishida, T. *Biochemistry* **2006**, *45*, 5413−5420. (c) Intharathep, P.; Tongraar, A.; Sagarik, K. *J. Comput. Chem.* **2006**, *27*, 1723−1732.

(4) Scheerder, J.; Vreekamp, R. H.; Engbersen, J. F. J.; Verboom, W.; van Duynhoven, J. P. M.; Reinhoudt, D. N. *J. Org. Chem.* **1996**, *61*, 3476−3481.

(5) Biali, S. E.; Böhmer, V.; Brenn, J.; Frings, M.; Thondorf, I.; Vogt, W.; Wohnert, J. *J. Org. Chem.* **1997**, *62*, 8350−8360.

(6) Dvořáková, H.; Šturša, J.; Čajan, M.; Moravcová, J. *Eur. J. Org. Chem.* **2006**, *19*, 4519−4527.

(7) Dvořáková, H.; Lang, J.; Vlach, J.; Sýkora, J.; Čajan, M.; Himl, M.; Pojarová, M.; Stibor, I.; Lhoták, P. *J. Org. Chem.* **2007**, *72*, 7157−7166.

(8) Kovalenko, V. I.; Chernova, A. V.; Borisoglebskaya, E. I.; Katsyuba, S. A.; Zverev, V. V.; Shagidullin, R. R.; Antipin, I. S.; Solov'eva, S. E.; Stoikov, I. I.; Konovalov, A. I. *Russ. Chem. Bull.* **2002**, *51*, 825−827.

(9) Gutsche, C. D.; Bauer, L. J. *J. Am. Chem. Soc.* **1985**, *107*, 6052−6059.

(10) Groenen, L. C.; Steinwender, R. E.; Lutz, B. T. G.; van der Maas, J. H.; Reindhout, D. N. *J. Chem. Soc., Perkin Trans. 2* **1992**, 1893−1898.

(11) Grootenhuis, P. D. J.; Kollman, P. A.; Groenen, L. C.; Reindhoudt, D. N.; van Hummel, G. J.; Ugozzoli, F.; Andreetti, G. D. *J. Am. Chem. Soc.* **1990**, *112*, 4165−4176.

(12) Fischer, S.; Grootenhuis, P. D. J.; Groenen, L. C.; van Hoorn, W. P.; van Veggel, F. C. J. M.; Reindhoudt, D. N.; Karplus, M. *J. Am. Chem. Soc.* **1995**, *117*, 1611−1620.

(13) Brougham, D. F.; Caciuffo, R.; Horsewill, A. J. *Nature* **1999**, *397*, 241−243.

(14) Horsewill, A. J.; Jones, N. H.; Caciuffo, R. *Science* **2001**, *291*, 100−103.

(15) Paolone, A.; Cantelli, R.; Caciuffo, R.; Arduini, A. *Phys. Rev. B* **2002**, *65*, 214−304.

(16) Lang, J.; Deckerová, V.; Czernek, J.; Lhoták, P. *J. Chem. Phys.* **2005**, *122*, 044056.

(17) Lang, J.; Vágnerová, K.; Czernek, J.; Lhoták, P. *Supramol. Chem.* **2006**, *18*, 371−381.

(18) Feyereisen, M.; Fitzgerald, G.; Komornicki, A. *Chem. Phys. Lett.* **1993**, *208*, 359−363.

(19) Alrichs, R.; Bar, M.; Haser, M.; Horn, H.; Kolmel, C. *Chem. Phys. Lett.* **1989**, *162*, 165−169.

(20) Frisch, M. J.; Trucks, G. W.; Schlegel, H. B.; Scuseria, G. E.; Robb, M. A.; Cheeseman, J. R.; Montgomery, J. A., Jr.; Vreven, T.; Kudin, K. N.; Burant, J. C.; Millam, J. M.; Iyengar, S. S.; Tomasi, J.; Barone, V.; Mennucci, B.; Cossi, M.; Scalmani, G.; Rega, N.; Petersson, G. A.; Nakatsuji, H.; Hada, M.; Ehara, M.; Toyota, K.; Fukuda, R.; Hasegawa, J.; Ishida, M.; Nakajima, T.; Honda, Y.; Kitao, O.; Nakai, H.; Klene, M.; Li, X.; Knox, J. E.; Hratchian, H. P.; Cross, J. B.; Bakken, V.; Adamo, C.; Jaramillo, J.; Gomperts, R.; Stratmann, R. E.; Yazyev, O.; Austin, A. J.; Cammi, R.; Pomelli, C.; Ochterski, J. W.; Ayala, P. Y.; Morokuma, K.; Voth, G. A.; Salvador, P.; Dannenberg, J. J.; Zakrzewski, V. G.; Dapprich, S.; Daniels, A. D.; Strain, M. C.; Farkas, O.; Malick, D. K.; Rabuck, A. D.; Raghavachari, K.; Foresman, J. B.; Ortiz, J. V.; Cui, Q.; Baboul, A. G.; Clifford, S.; Cioslowski, J.; Stefanov, B. B.; Liu, G.; Liashenko, A.; Piskorz, P.; Komaromi, I.; Martin, R. L.; Fox, D. J.; Keith, T.; Al-Laham, M. A.; Peng, C. Y.; Nanayakkara, A.; Challacombe, M.; Gill, P. M. W.; Johnson, B.; Chen, W.; Wong, M. W.; Gonzalez, C.; Pople, J. A. *Gaussian 03*, revision C.02; Gaussian, Inc.: Wallingford, CT, 2004.

(21) Čajan, M.; Lhoták, P.; Lang, J.; Dvořáková, H.; Stibor, I.; Koča, J. *J. Chem. Soc., Perkin Trans. 2* **2002**, *11*, 1922−1929.

(22) Matoušek, J.; Kulhánek, P.; Čajan, M.; Koča, J. *J. Phys. Chem. A* **2006**, *110*, 861−867.

(23) (a) Weigend, F.; Häser, M.; Patzelt, H.; Ahlrichs, R. *Chem. Phys. Lett.* **1998**, *294*, 143−152. (b) Weigend, F.; Köhn, A.; Hättig, C. *J. Chem. Phys.* **2001**, *116*, 3175−3183. (c) Jurečka, P.; Nachtigall, P.; Hobza, P. *Phys. Chem. Chem. Phys.* **2001**, *3*, 4578−4582. (d) Braun, J.; Neusser, H. J.; Hobza, P. *J. Phys. Chem. A* **2003**, *107*, 3918−3924.

(24) Klamt, A.; Schüürmann, G. *J. Chem. Soc., Perkin Trans. 2* **1993**, *5*, 799−805.

(25) Fernandez-Ramos, A.; Smedarchina, Z.; Pichierri, F. *Chem. Phys. Lett.* **2001**, *343*, 627−632.